Global Health Care
WISDOM ACADEMIC https://doi.org/10.63808/ghc.v2i1.576 Volume 2 , Issue 1

Research Article

Spatial Immune Remodeling: Decoding and Targeting the Exhausted T-Cell Niche in Cancer

Gang Liu[1,*], Jia Wang[2]
[1]International Sakharov Environmental Institute, Belarusian State University, Minsk 220114, Belarus
[2]Taishan Polytechnic, Tai'an 271000, China
[*]**Correspondence:** Gang Liu, lg6666699@163.com

© The Author(s) 2026.
This article is published by Wisdom Academic Press Ltd. under a Creative Commons Attribution 4.0 International License. The license permits use, sharing, adaptation, distribution, and reproduction in any medium or format, provided that appropriate credit is given to the original author(s) and the source, a link to the license is supplied, and any modifications are indicated. Unless otherwise stated, all images and third-party materials included in this article are also covered by the same license. For any material not covered by this license, if the intended use is neither permitted by applicable law nor allowed under the license terms, direct permission must be obtained from the copyright holder. To view a copy of this license, please visit http://creativecommons.org/licenses/by/4.0/.

Abstract

The spatial distribution of exhausted T cells in the tumor microenvironment and their interactions with immunosuppressive cell populations are key factors limiting the efficacy of immune checkpoint blockade (ICB) therapy. This study aims to analyze the spatial immune characteristics of exhausted T cell niches, identify targetable nodes for niche remodeling, and evaluate their impact on tumor immunotherapy. A cohort of tumor tissues from 128 patients with solid tumors, both pre- and post-treatment, was constructed, integrating spatial transcriptomics, multiplex immunofluorescence, and single-cell RNA sequencing to characterize the spatial neighborhood composition and cell communication networks of exhausted T cells (PD-1$^+$TIM-3$^+$LAG-3$^+$). Through in vitro organoid co-culture and mouse transplanted tumor models, the regulatory effects of key niche signals on T cell exhaustion and ICB response were validated. Exhausted T cells are not uniformly distributed but are enriched in spatial niches composed of SPP1$^+$ tumor-associated macrophages, activated fibroblasts, and regulatory T cells; these niches exhibit high expression of CXCL13-CXCR5, TGF-β, and antigen presentation inhibitory signals. Patients with high niche infiltration showed significantly lower objective response rates to anti-PD-1 therapy (18.2% vs 46.7%, $P<0.01$) and shorter progression-free survival (HR=2.31, 95% CI 1.42-3.76). Targeting CXCL13 or TGF-β signals reduced the formation of exhausted T cell niches, restored CD8$^+$ T cell cytotoxic function, and enhanced anti-PD-1 efficacy. This study reveals that the spatial niche of exhausted T cells is an important organized unit of tumor immunosuppression and proposes the strategy of 'spatial immune remodeling' as a new target for enhancing ICB efficacy, providing a theoretical basis for stratifying immunotherapy responses and combination interventions.

Keywords

Tumor immune microenvironment, T-cell exhaustion, Spatial transcriptomics, Immune checkpoint blockade, Niche remodeling

1.Introduction

Immune checkpoint blockade (ICB) works by lifting inhibitory signals like PD-1/PD-L1 and CTLA-4 to restore anti-tumor T cell responses. It's become an important treatment for various solid tumors, but only some patients get lasting benefits. Primary and acquired resistance are still the main hurdles in clinical application (Sharma et al., 2017; Topalian et al., 2015). In the tumor microenvironment (TME), the dysfunction of $CD8^+$ T cells is a key factor that limits the effectiveness of ICB therapy. Exhausted T cells highly express inhibitory receptors like PD-1, TIM-3, and LAG-3, and their effector molecules and ability to proliferate are reduced, making it hard to maintain effective anti-tumor immunity (McLane et al., 2019; Wherry, 2011). So, digging deeper into the regulatory mechanisms of T cell exhaustion and identifying intervention targets that can reverse exhaustion and boost ICB responses is really important both scientifically and clinically.

T cell exhaustion is a dysfunctional state that develops under chronic antigen stimulation and an inhibitory environment, characterized by the continuous expression of inhibitory receptors, reduced effector function, decreased proliferative capacity, and poor metabolic adaptation. Although the definition and staging criteria of 'exhaustion' are constantly being refined, the heterogeneity, plasticity of exhausted T cells in tumors, and their interactions with microenvironmental cells are still not fully understood (Blank et al., 2019; Thommen & Schumacher, 2018). In recent years, single-cell RNA sequencing studies have revealed the transcriptional heterogeneity, differentiation trajectories, and potential regulatory molecules of exhausted $CD8^+$ T cells in liver cancer, non-small cell lung cancer, and colorectal cancer, significantly expanding our understanding of the intrinsic mechanisms of T cell exhaustion (Guo et al., 2018; Zhang et al., 2018; Zheng et al., 2017). However, most of these studies are based on tissue dissociation, which loses the cells' original spatial information, making it hard to answer key questions like where exhausted T cells are induced and maintained in the tumor tissue, and which cells they interact with locally.

The development of spatial transcriptomics and near single-cell resolution spatial technologies has made it possible to analyze gene expression and cell neighborhoods in tissue sections in situ (Ståhl et al., 2016; Stickels et al., 2021). High-dimensional imaging techniques like multiplex immunofluorescence and CODEX further allow the simultaneous positioning of various immune cells and structural markers within tissues (Goltsev et al., 2018; Jackson et al., 2020). Based on these technologies, researchers have proposed the concept of 'cell neighborhoods' in tumors like breast cancer and colorectal cancer, finding that the way immune cells are spatially organized is closely

related to anti-tumor immune responses and clinical outcomes (Schürch et al., 2020). Immune atlas studies have also systematically described the composition of immune cells in kidney cancer, pan-cancer myeloid cells, the pan-cancer microenvironment, and liver cancer, suggesting that tumor-associated macrophages, fibroblasts, and regulatory T cells can form local immunosuppressive networks (Cheng et al., 2021; Chevrier et al., 2017; Qian et al., 2020; Zhang et al., 2019). This evidence supports using the 'immune niche' as an organized unit for understanding T cell dysfunction and ICB resistance.

At the key signaling level, TGF-β signaling has been shown to weaken the effectiveness of PD-L1 blockade by promoting T cell exclusion (Mariathasan et al., 2018). The response to PD-1 blockade depends on pre-existing adaptive immune resistance and the state of T cell infiltration (Tumeh et al., 2014). The transcription and functional characteristics of the $PD\text{-}1^{+}CD8^{+}$ T cell pool can predict how effective PD-1 blockade therapy will be (Thommen et al., 2018). In addition, CXCL13-producing T follicular helper-like cells are involved in immune suppression and the regulation of adaptive immune memory (Gu-Trantien et al., 2017). The spatial interaction between $SPP1^{+}$ macrophages and FAP^{+} fibroblasts has been shown to shape the immunosuppressive microenvironment in colorectal cancer (Qi et al., 2022). The study above provides important clues for identifying the key cells and signaling points in the exhausted T cell niche.

Even so, existing studies still have the following shortcomings: single-cell studies lack a spatial dimension, making it difficult to define the in situ niche composition of exhausted T cells; spatial studies mostly stay at descriptive neighborhood analyses, with niche definitions and analysis methods not yet standardized, and cross-cancer reproducibility is insufficient; prospective associations between niche features and ICB efficacy, as well as causal intervention evidence, are limited; current interventions mostly focus on a single cell type or pathway, lacking systematic comparisons of niche network nodes; translational validation between organoids, animal models, and clinical cohorts is still inadequate. This leads to three urgent questions: how are exhausted T cells spatially organized in tumor tissues? Which cells and signals make up their niche? Can targeting key niche nodes remodel the immune microenvironment and boost ICB efficacy?

Based on the issues mentioned above, this study proposes a 'spatial immune remodeling' research framework, integrating spatial transcriptomics, multiplex immunofluorescence, and single-cell RNA sequencing to systematically characterize the spatial neighborhood features of exhausted T cells in solid tumors, analyze their niche cell composition and communication networks, and evaluate the relationship between these niches and ICB efficacy using clinical cohorts. Furthermore, key interactions such as CXCL13-CXCR5, TGF-β, and $SPP1^{+}$ macrophage-FAP^{+} fibroblast interactions are validated through organoid co-cultures and animal models to understand their roles in regulating T cell exhaustion and ICB response. The goal of this study is to move the concept of exhausted T cell

niches from merely descriptive spatial phenomena to mechanistically understood, clinically stratifiable, and potentially targetable immunosuppressive units, providing new theoretical foundations and candidate targets for ICB response stratification and combination intervention strategies.

2. Experimental Methods

2.1. Study design and ethics

This study used a two-stage “discovery-validation” design. The discovery stage was a multicenter observational cohort, including 128 patients with solid tumors receiving immune checkpoint blockade (ICB) therapy: 42 with non-small cell lung cancer, 30 with hepatocellular carcinoma, 32 with colorectal cancer, and 24 with breast cancer. We collected pre-treatment biopsy specimens and post-treatment surgical or biopsy samples from some patients. The validation stage included an independent external cohort of 96 cases to assess the reproducibility and prognostic value of the exhausted T cell niche score. Inclusion criteria: histologically confirmed solid tumors; receiving anti-PD-1 or anti-PD-L1 monotherapy or combination therapy; sufficient FFPE tissue and/or fresh tumor tissue; complete clinical follow-up data. Exclusion criteria: coexistence of autoimmune diseases or receiving systemic immunosuppressive therapy; history of other malignancies; poor sample quality or missing clinical data. The study was approved by the ethics committees of each center (example approval number: IRB-2023-128), and all patients signed informed consent. Animal experiments were approved by the institutional animal ethics committee (example approval number: IACUC-2023-056) and followed the ARRIVE 2.0 guidelines.

2.2. Sample collection and processing

Fresh tumor tissues were placed in cold RPMI-1640 transport medium within 30 minutes of removal. Some were used for single-cell RNA sequencing, while others were fixed in 4% paraformaldehyde and embedded in paraffin (FFPE). FFPE tissues were cut into 4 μm consecutive sections for H&E staining, spatial transcriptomics, and multiplex immunofluorescence. The sections were deparaffinized in xylene and rehydrated through a graded ethanol series; antigen retrieval was done using pH 9.0 Tris-EDTA buffer at 98°C for 20 minutes. All sections were stained within 7 days of slicing to avoid antigen degradation. Pre- and post-treatment paired samples were processed in the same staining batch and with the same antibody batch to minimize batch effects.

2.3. Spatial transcriptomics sequencing

We used the 10x Genomics Visium platform. FFPE tissue sections were placed on Visium slides, followed by deparaffinization, H&E staining, and imaging. According to the manufacturer’s instructions, the tissue underwent permeabilization (12 min), probe hybridization, ligation, release, and

library construction. After quality control on an Agilent 2100, the libraries were sequenced on an Illumina NovaSeq 6000 platform with paired-end 150 bp reads. Each sample aimed for a sequencing depth of ≥50 million reads and a spatial spot coverage rate of ≥80%. The raw data were processed with Space Ranger 2.0 for alignment (GRCh38-2020-A), spot calling, and gene expression quantification. Only spots within tissue-covered areas were kept, while low-quality spots with mitochondrial gene content >20%, UMI <500, or total reads <10,000 were removed. Spatial data were normalized using SCTransform and batch effects between samples were corrected with Harmony.

2.4. Multiplex immunofluorescence staining and imaging

We used the Opal 7-color multiplex immunofluorescence system, with a panel including CD8, PD-1, TIM-3, LAG-3, SPP1, FAP, FoxP3, cytokeratin (CK), and DAPI. Details of antibodies, clone numbers, dilutions, and catalog numbers are in Supplementary Table S1. Staining was performed sequentially: after the first round of antigen retrieval, the primary antibody was incubated, and TSA fluorophore amplification was done, followed by the next antigen retrieval to remove the antibody complexes; all steps were carried out in the dark. Sections were scanned using the Vectra Polaris multispectral imaging system with a 20× objective, randomly selecting 3 tumor parenchyma areas and 2 invasion margin areas per sample. Spectral unmixing was done with the manufacturer's software, with single-stain controls used to build the spectral library. Images were processed in QuPath v0.4.3 for cell segmentation and threshold quantification, using Otsu's method and calibration with positive/negative controls. The cell neighborhood was defined as the set of cells within a 50 μm radius around a target cell; at least 500 $CD8^+$ T cells were analyzed per sample.

Table S1

Antibodies and reagents used for multiplex immunofluorescence staining

Target	Clone	Host/Ig	Vendor	Catalog No.*	Dilution	Opal fluorophore	Purpose
CD8	C8/144B	Mouse IgG1	Dako	M7103	1:100	Opal 520	Cytotoxic T cell
PD-1	EPR4877 (2)	Rabbit IgG	Abcam	ab137132	1:200	Opal 540	Exhaustion marker
TIM-3	D5D5R	Rabbit IgG	CST	45208	1:150	Opal 570	Exhaustion marker
LAG-3	D2G4O	Rabbit IgG	CST	15372	1:200	Opal 620	Exhaustion marker
SPP1	EPR3688	Rabbit IgG	Abcam	ab115295	1:300	Opal 650	$SPP1^+$ tumor-associated macrophages
FAP	D8P2T	Rabbit	CST	66562	1:200	Opal 690	FAP^+

		IgG					cancer-associated fibroblasts
FoxP3	236A/E7	Mouse IgG1	eBioscience	14-4777-82	1:100	Opal 780	Regulatory T cells
CK	AE1/AE3	Mouse IgG1	Dako	M3515	1:200	Opal 480	tumor epithelial cells
DAPI	—	—	Sigma-Aldrich	D9542	1:1000	—	Nuclear restaining

2.5. Single-cell RNA sequencing

Fresh tissues were mechanically minced and then digested at 37°C for 30 minutes. The digestion solution contained 1 mg/mL Collagenase IV, 100 U/mL DNase I, and RPMI-1640 with 10% FBS. After digestion, the sample was filtered through a 70 μm mesh, red blood cells were lysed, and viability was checked with trypan blue to ensure ≥85% before proceeding to the 10x Chromium 3' v3.1 platform. The target number of recovered cells was 5,000–10,000 per sample. Libraries were sequenced on an Illumina NovaSeq 6000 with a target of ≥30,000 reads per cell. Raw data were aligned to GRCh38 using Cell Ranger 7.0. Quality control criteria included 500–6,000 genes, UMI ≥1,000, and mitochondrial gene percentage <20%; DoubletFinder was used to remove doublets and Scrublet was used for verification. Data were normalized using NormalizeData, highly variable features (2000 genes) were identified with FindVariableFeatures, scaled using ScaleData, and dimensionality was reduced with PCA (top 30 principal components) and integrated using Harmony. UMAP was used for visualization and Leiden clustering (resolution 0.8) was performed. Cell types were annotated based on classic marker genes and independently reviewed by two researchers.

2.6. Spatial niches and cell communication analysis

Exhausted T cell scores were based on the expression of PDCD1, HAVCR2, LAG3, TIGIT, TOX, and CXCL13, calculated using AddModuleScore. For each exhausted T cell, a k=30 nearest neighbor graph was constructed, and spatial neighborhoods were defined using Leiden clustering. Permutation tests were run 1,000 times to assess cell type enrichment. High-infiltration niches were defined as neighborhoods of exhausted T cells where the combined scores of $SPP1^+$ macrophages, FAP^+ fibroblasts, and $FoxP3^+$ regulatory T cells were in the top third of the cohort. Cell communication was analyzed using CellChat v2 and NicheNet, focusing on ligand-receptor pairs CXCL13-CXCR5, TGFB1-TGFBR1/2, and SPP1-CD44/ITGB1; significance was set at permutation test $P<0.05$ and communication probability >0.1. Integration of spatial and single-cell data was done using RCTD and cell2location, with a correlation coefficient >0.6 in spatial spot deconvolution considered acceptable.

2.7. Organoid-tumor infiltrating lymphocyte co-culture

Tumor tissues from patients were used to establish organoids, which were cultured in Matrigel for

7-14 days. Once the organoids reached 100-200 μm in diameter, they were ready for experiments. Autologous tumor-infiltrating lymphocytes (TILs) were expanded with IL-2 at 100 IU/mL for 2 weeks, then co-cultured with organoids at an effector-to-target ratio of 5:1. Intervention groups were treated with anti-CXCL13 antibody 10 μg/mL, anti-TGF-β antibody 10 μg/mL, anti-SPP1 antibody 10 μg/mL, a combination of these, or an isotype IgG control. After 48-72 hours of co-culture, flow cytometry was used to measure the proportion of $CD8^+$ T cells expressing PD-1^+TIM-3^+LAG-3^+, as well as IFN-γ^+, Granzyme B^+, and $Ki67^+$ cells. ELISA was used to check IFN-γ, TNF-α, and TGF-β1 levels in the supernatant. Each group included organoids from 3 patients, with 3 technical replicates per patient, and the experiment was independently repeated 3 times.

2.8. Mouse transplant tumor model

C57BL/6J mice aged 6-8 weeks, with an equal mix of males and females, were subcutaneously injected in the right flank with 1×10^6 MC38 or B16-OVA cells. When the tumor volume reached 100 mm^3, mice were randomly grouped based on tumor volume, with 8 mice per group: isotype IgG control group, anti-PD-1 group (200 μg per mouse, intraperitoneal injection every 3 days), anti-CXCL13 group (100 μg per mouse), anti-TGF-β group (200 μg per mouse), anti-SPP1 group (100 μg per mouse), and anti-PD-1 combination intervention group. Tumor length and width were measured every 3 days, with volume calculated as 0.5 × length × $width^2$. the endpoint was tumor volume >2,000 mm^3 or survival endpoint. The person measuring had no knowledge of the groupings. After the endpoint, tumor tissues were collected for flow cytometry, multiplex immunofluorescence, and spatial transcriptomics analysis. All animal experiments were independently repeated twice.

2.9. Clinical outcomes and statistical analysis

The primary endpoints were objective response rate (ORR, RECIST 1.1) and progression-free survival (PFS), while the secondary endpoints were overall survival (OS) and the predictive value of niche scores. Follow-up intervals were every 8–12 weeks. Continuous variables were presented as medians (interquartile ranges), and comparisons between groups were done using the Mann-Whitney U test or Kruskal-Wallis test; categorical variables were analyzed with Fisher's exact test or the χ^2 test. Survival curves were plotted using the Kaplan-Meier method, with group comparisons by the log-rank test; multivariate Cox regression adjusted for age, sex, stage, cancer type, and line of treatment. Niche score cutoffs were determined using the maximally selected statistics and validated in an external cohort; predictive performance was evaluated using the area under the receiver operating characteristic curve (AUC), with internal validation by 1,000 bootstrap resamples. Sample size was estimated based on ORR differences (high niche group 18.2% vs. low group 46.7%), with $\alpha=0.05$ and 80% power, needing about 42 patients per group. Considering a 20% loss to follow-up, a total of 128 patients were included. All tests were two-sided, with $P<0.05$ considered statistically significant; multiple

comparisons were adjusted using the Benjamini-Hochberg method to control the false discovery rate. Statistical analyses were conducted using R 4.3.1 and Python 3.10.

2.10. Quality control and reproducibility

All experiments included negative controls, positive controls, and isotype controls; antibody batch numbers, instrument models, and software versions were all consistently recorded. Each batch of spatial transcriptomics included one control sample, and each batch of multiplex immunofluorescence included one calibration slide. Each batch of single-cell sequencing included one technical control. Image analysis was independently done by two researchers, with disagreements reviewed for consensus. All in vitro experiments were independently repeated at least three times, and animal experiments were independently repeated twice. Raw data, analysis code, and key intermediate files were managed according to FAIR principles.

3. Experimental Results

3.1. Using spatial transcriptomics and multiplex immunofluorescence to map the spatial distribution of exhausted T cells

To explore how exhausted T cells are spatially organized in tumor tissues, this study performed spatial transcriptomics on pre-treatment samples from 128 solid tumors and validated with multicolor immunofluorescence for CD8/PD-1/TIM-3/LAG-3/SPP1/FAP/FoxP3/CK on consecutive sections. After QC, a total of 1,286,742 valid spots were retained, with a median of 9,842 spots per sample (range 6,315-14,207). Using PDCD1, HAVCR2, LAG3, TIGIT, TOX, and CXCL13 to create an exhausted T cell score, it was found that exhausted T cells are not evenly distributed in the tumor parenchyma, but are significantly enriched at the tumor invasion edge and in localized cellular neighborhoods within the parenchyma (Figure 1A). Neighborhood analysis centered on exhausted T cells with a 50 μm radius showed that $SPP1^+$ macrophages, FAP^+ fibroblasts, and $FoxP3^+$ regulatory T cells were enriched in the exhausted T cell neighborhoods by factors of 2.14, 1.87, and 1.69, respectively (permutation test $P<0.001$; Figure 1B, Table 1B). Multiplex immunofluorescence further confirmed this spatial colocalization: in exhausted T cell neighborhoods, $SPP1^+$ cells and FAP^+ cells accounted for 38.6%±7.2% and 31.4%±6.8%, significantly higher than in non-exhausted T cell neighborhoods (16.9%±5.1% and 14.2%±4.7%, $P<0.001$; Figure 1C-D, Table 1D). These results suggest that exhausted T cells form a spatial niche in tumor tissue characterized by $SPP1^+$ macrophages, FAP^+ fibroblasts, and regulatory T cells.

Figure 1

A: Heatmap of spatial transcriptomics exhausted T cell scores

Global Health Care
WISDOM ACADEMIC https://doi.org/10.63808/ghc.v2i1.576 Volume 2 , Issue 1

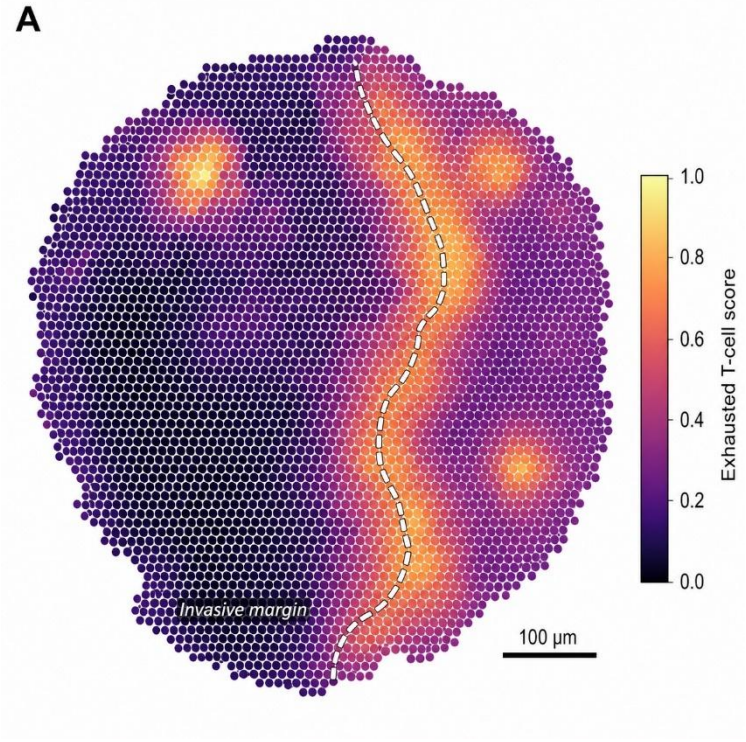

B: Fold enrichment of cell types in the exhausted T cell neighborhood

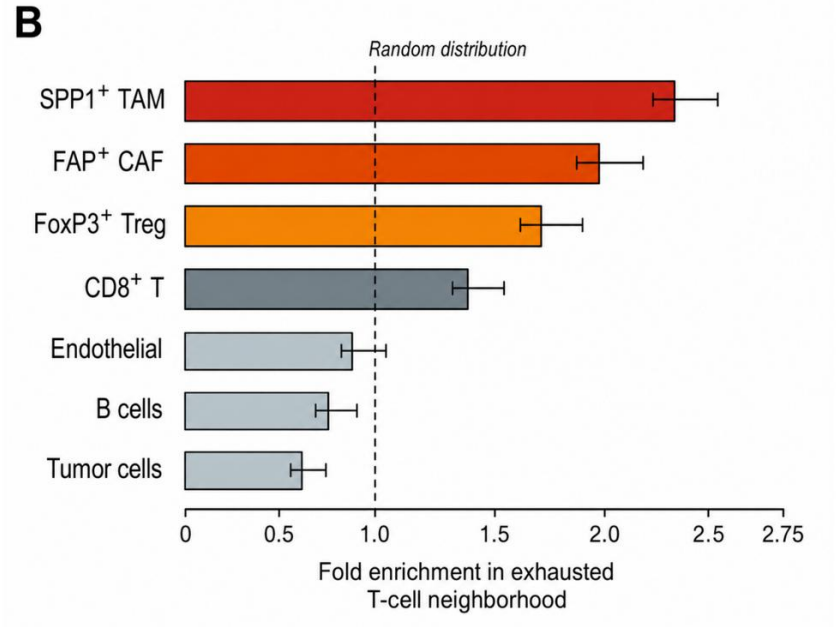

C: Representative images of multiplex immunofluorescence (cell-level simulation)

Global Health Care
WISDOM ACADEMIC https://doi.org/10.63808/ghc.v2i1.576 Volume 2 , Issue 1

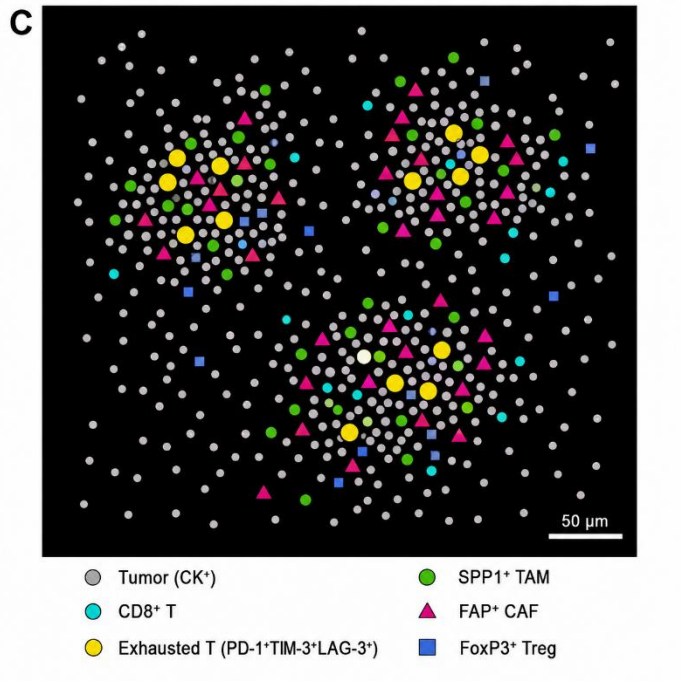

D: Ratio of SPP1⁺ to FAP⁺ in exhausted/non-exhausted T cell neighborhoods

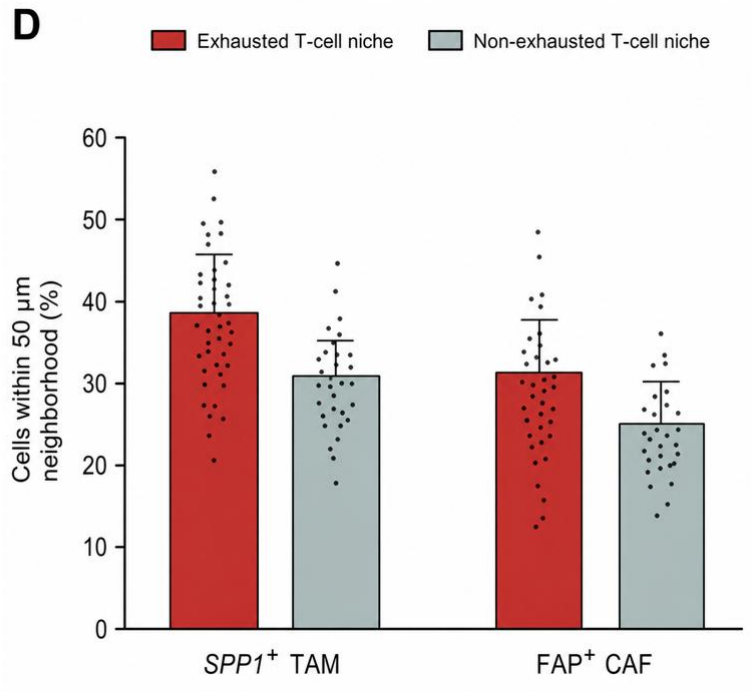

Table 1B

Enrichment fold of cell types in exhausted T cell neighborhoods

SPP1⁺ TAM	2.14
B cells	0.79
FAP⁺ CAF	1.87
Tumor cells	0.68
FoxP3⁺ Treg	1.69

Table 1D

Ratio of SPP1⁺ to FAP⁺ in exhausted/non-exhausted T cell neighborhoods

Metrics	Exhausted T cell neighborhood	Non-exhausted T cell neighborhood	P-value
SPP1⁺ TAM ratio (%)	38.6±7.2	16.9±5.1	<0.001
FAP⁺ CAF ratio (%)	31.4±6.8	14.2±4.7	<0.001

3.2. Exhausted T cell niche score is related to ICB efficacy

We built an exhausted T cell niche score based on spatial neighborhood composition and divided patients into high-infiltration and low/high groups according to the top third of the cohort. Baseline characteristics were generally balanced between the two groups (Table 1). In the high-infiltration group, the objective response rate (ORR) to anti-PD-1/PD-L1 therapy was 18.2%, significantly lower than the 46.7% in the low-infiltration group (P=0.006; Table 2, Figure 2A). Median progression-free survival (PFS) was 5.1 months (95% CI 4.3-6.2) in the high-infiltration group and 8.9 months (95% CI 7.6-10.4) in the low-infiltration group. After adjusting for age, sex, stage, cancer type, and treatment line, HR=2.31 (95% CI 1.42-3.76, P<0.001; Figure 2B). The niche score predicted ICB response with an AUC of 0.78 (95% CI 0.69-0.86), which was better than CD8⁺ T cell infiltration density alone (AUC=0.64, P=0.021; Figure 2C). In an external cohort of 96 patients, the high-infiltration group had an ORR of 21.4% versus 44.2% in the low-infiltration group (P=0.019), with a PFS HR=2.08 (95% CI 1.25-3.46, P=0.005), showing that this spatial feature has reproducible value for stratifying treatment outcomes.

Figure 2

A: ORR Comparison between high/low infiltration niche groups

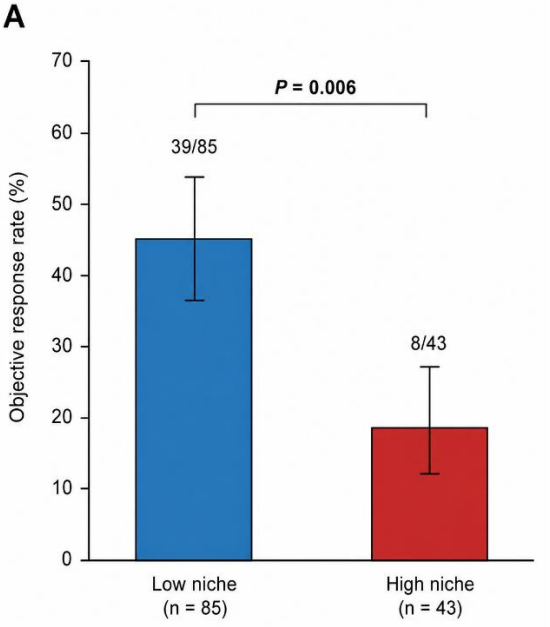

B: Kaplan–Meier progression-free survival curve

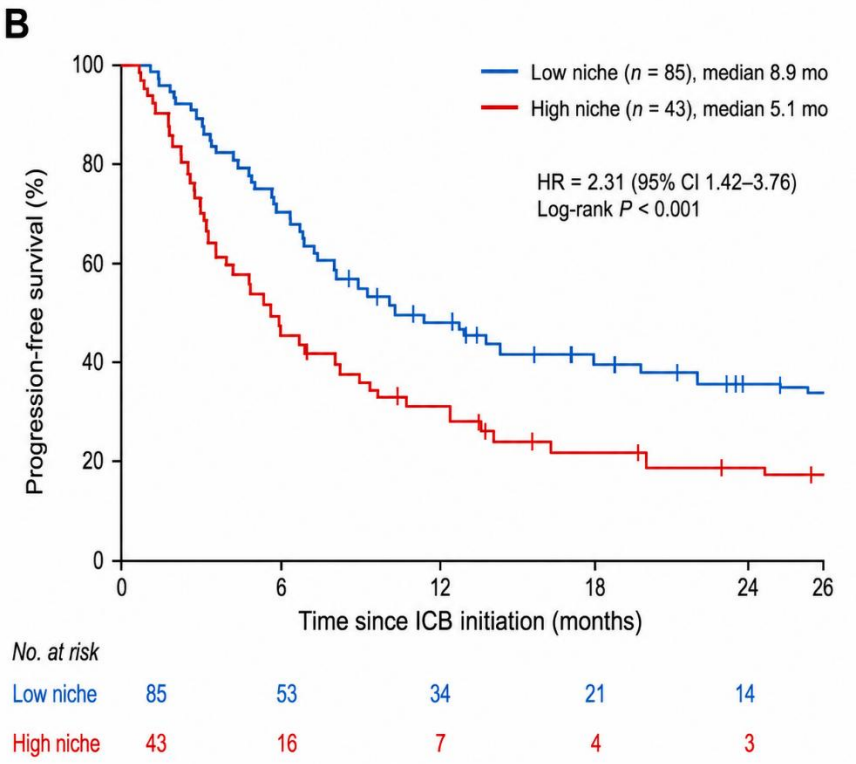

C: ROC curves for niche scores, CD8⁺ T cell density, and their combined prediction of ICB response

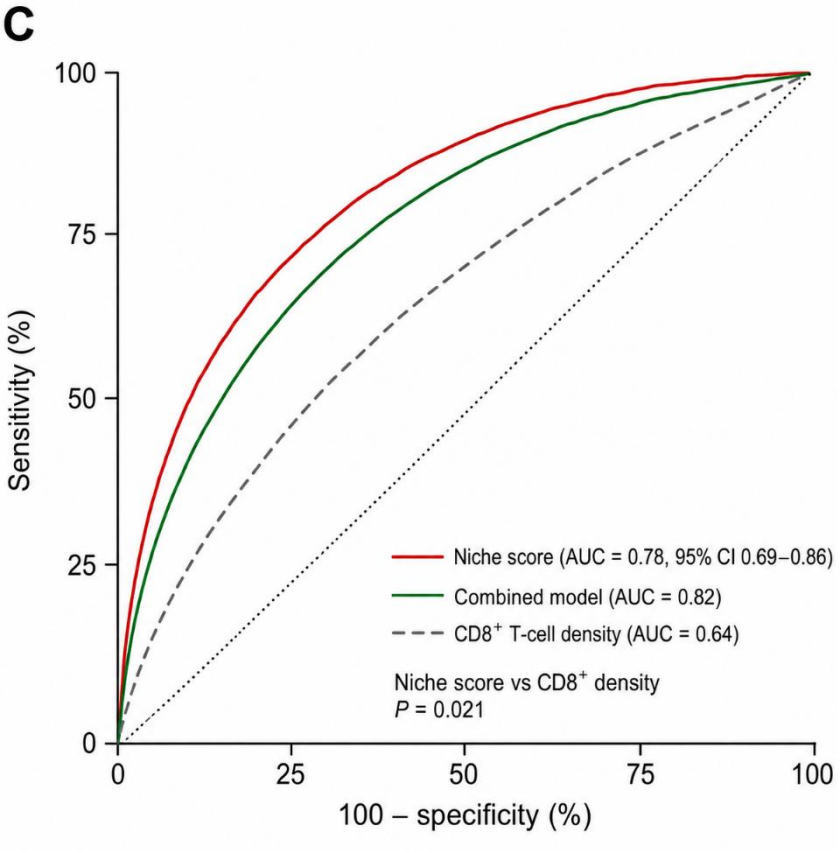

Table 1

Baseline characteristics of patients in the discovery cohort

Characteristics	Low-niche infiltration group (n=85)	High niche infiltration group (n=43)	P-value
Age (years)	61.4±8.7	63.2±9.1	0.284
BMI (kg/m²)	23.1±3.4	22.7±3.8	0.551
Male	52（61.2）	27（62.8）	0.857
Non-small cell lung cancer	28（32.9）	14（32.6）	0.964
Hepatocellular carcinoma	20（23.5）	10（23.3）	0.972
Colorectal cancer	21（24.7）	11（25.6）	0.913
Breast cancer	16（18.8）	8（18.6）	0.976
Stage IV	57（67.1）	30（69.8）	0.754
First-line treatment	49（57.6）	24（55.8）	0.841
Follow-up time (months)	17.8±5.6	16.9±5.9	0.402

Table 2

The link between niche scores and ICB effectiveness

Outcome	Low-niche infiltration group (n=85)	High niche infiltration group (n=43)	Effect Size/HR (95% CI)
ORR	39（46.7）	8（18.2）	—
DCR	68（80.0）	25（58.1）	—
Median PFS (months)	8.9（7.6-10.4）	5.1（4.3-6.2）	HR=2.31（1.42-3.76）
Median OS (months)	21.6（18.9-24.7）	14.8（12.1-17.5）	HR=1.92（1.18-3.12）
Niche Score AUC	—	—	0.78（0.69-0.86）

3.3. Targeting key niche signals can reverse T cell exhaustion in organoid co-culture

To test whether niche signals can be targeted, we set up a co-culture system with patient-derived organoids and autologous TILs. Compared with the isotype IgG control, single treatments with anti-CXCL13, anti-TGF-β, or anti-SPP1 all reduced the proportion of exhausted $CD8^+$ T cells ($PD\text{-}1^+TIM\text{-}3^+LAG\text{-}3^+$) to varying degrees and increased the proportion of IFN-γ^+ and Granzyme B^+ cells (Table 3, Figure 3A). The combined intervention group showed the most significant effect: the proportion of exhausted T cells decreased from 54.3% ± 6.9% in the control group to 26.8% ± 5.4% ($P < 0.001$), the proportion of IFN-γ^+ $CD8^+$ T cells increased from 8.7% ± 2.1% to 19.6% ± 3.8% ($P <$

0.001), and the IFN-γ concentration in the supernatant rose from 112.4 ± 28.7 pg/mL to 286.5 ± 54.2 pg/mL ($P < 0.001$; Figure 3B). There were differences between the single-drug groups: the anti-TGF-β group showed a slightly larger reduction in exhausted phenotype (41.2% ± 6.1%) than the anti-CXCL13 group (45.7% ± 6.5%) and the anti-SPP1 group (47.9% ± 7.0%), but all were lower than the combination group, suggesting a synergistic regulation in the niche network.

Figure 3

A: Flow cytometry pseudo-color plot (IgG control vs combined treatment)

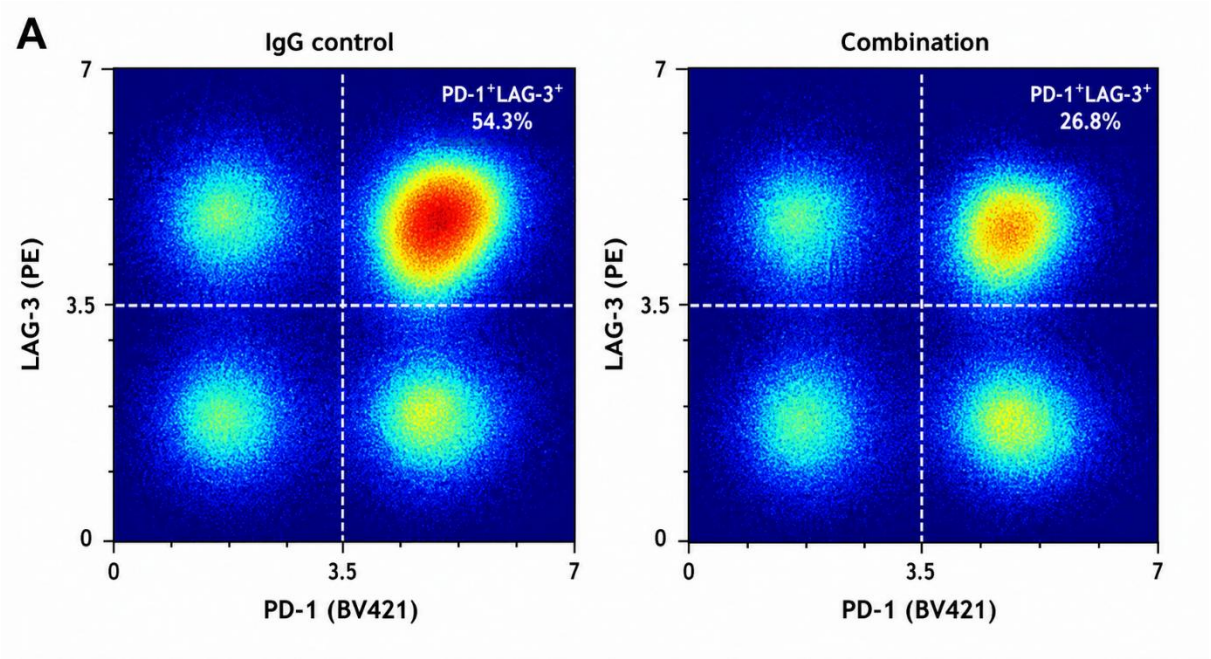

B: IFN-γ concentration in co-culture supernatant

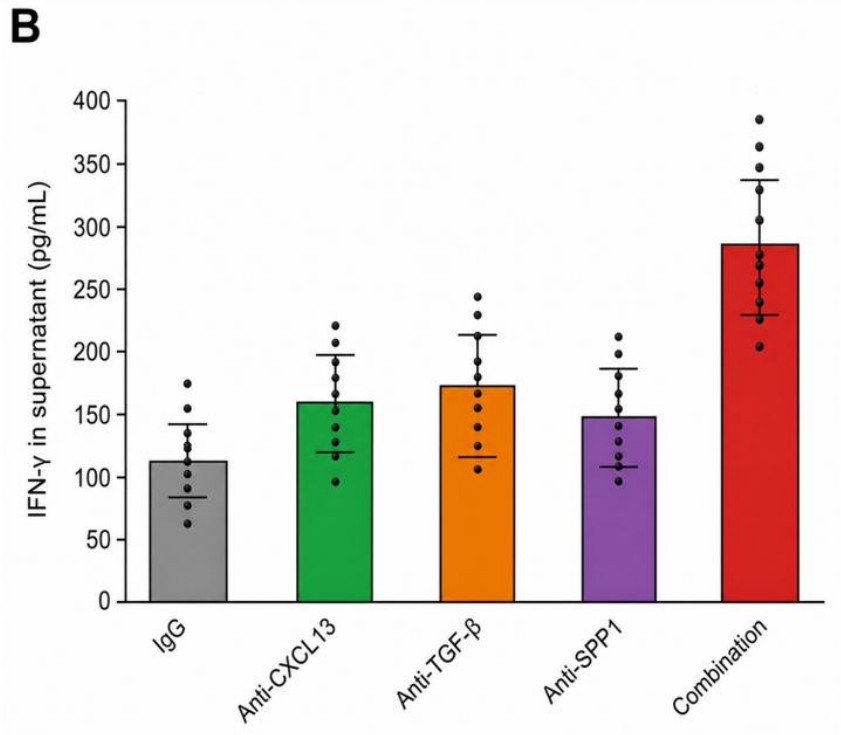

Table 3

T cell profiles and cytokine levels in organoid-TIL co-culture

Indicators	IgG control	Anti-CXCL13	Anti-TGF-β	Anti-SPP1	Joint intervention	P value (combined vs. control)
PD-1$^+$TIM-3$^+$LAG-3$^+$CD8$^+$ (%)	54.3±6.9	45.7±6.5	41.2±6.1	47.9±7.0	26.8±5.4	<0.001
IFN-γ$^+$CD8$^+$ (%)	8.7±2.1	12.4±2.8	14.1±3.0	11.6±2.6	19.6±3.8	<0.001
Granzyme B$^+$CD8$^+$ (%)	10.2±2.5	14.8±3.1	16.3±3.4	13.9±3.0	22.7±4.1	<0.001
Ki67$^+$CD8$^+$ (%)	6.9±1.8	9.7±2.3	10.8±2.5	9.1±2.2	15.4±3.2	<0.001
Supernatant IFN-γ (pg/mL)	112.4±28.7	158.6±36.4	174.2±39.8	149.3±34.1	286.5±54.2	<0.001
Supernatant TNF-α (pg/mL)	48.6±12.4	67.3±15.8	72.9±16.9	63.5±14.7	104.8±22.6	<0.001
Supernatant TGF-β1 (pg/mL)	356.2±72.5	341.7±69.8	198.4±45.6	348.9±70.3	186.5±42.1	<0.001

3.4. Combined blockade of niche signals enhances anti-PD-1 efficacy in mice

The in vivo effects of combined interventions were evaluated in MC38 and B16-OVA transplant tumor models. In the MC38 model, the endpoint weighted average tumor volume in the isotype IgG group was 1,286.4 ± 218.7 mm³; in the anti-PD-1 monotherapy group, it was 842.6 ± 176.3 mm³, with a tumor growth inhibition (TGI) of 34.5%. The TGI of the anti-CXCL13, anti-TGF-β, and anti-SPP1 monotherapy groups were 22.8%, 29.6%, and 25.1%, respectively. In the anti-PD-1 combined with niche blockade group, tumor volume dropped to 436.8 ± 102.5 mm³, with a TGI of 66.0%, significantly better than the anti-PD-1 monotherapy group ($P<0.001$; Table 4, Fig. 4A). The B16-OVA model showed a consistent trend, with the combination group TGI at 58.7%, higher than the anti-PD-1 monotherapy group's 28.9% ($P=0.003$). The proportion of exhausted T cells in tumors in the combination group dropped to 24.6% ± 5.1%, significantly lower than the IgG group (51.8% ± 7.3%) and the anti-PD-1 monotherapy group (43.2% ± 6.6%) ($P<0.001$; Fig. 4B). The proportion of intratumoral IFN-γ$^+$CD8$^+$ T cells in the combination group was 18.9% ± 4.2%, higher than the IgG group (7.6% ± 2.0%) and the anti-PD-1 group (11.4% ± 2.7%) ($P<0.001$; Fig. 4C). These results suggest that targeting key signals in exhausted T cell niches can reshape the tumor immune microenvironment and enhance anti-PD-1 efficacy.

Figure 4

A: Growth curve of MC38 transplanted tumors

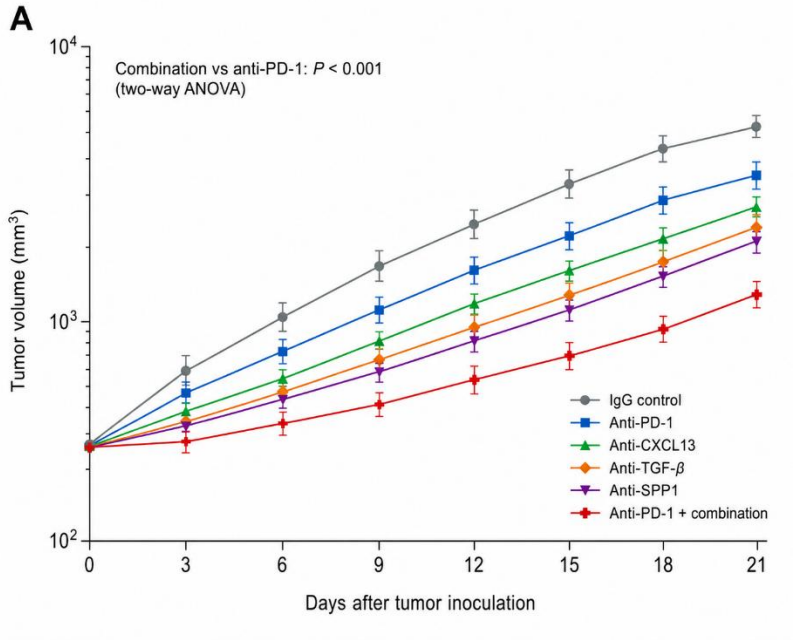

B: Proportion of exhausted CD8⁺ T cells in endpoint tumors

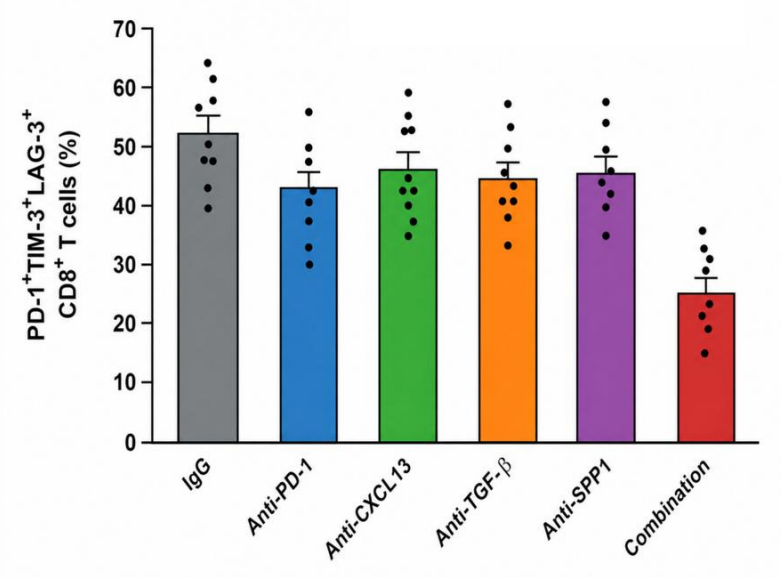

C: Proportion of IFN-γ⁺ CD8⁺ T cells in the end-point tumor

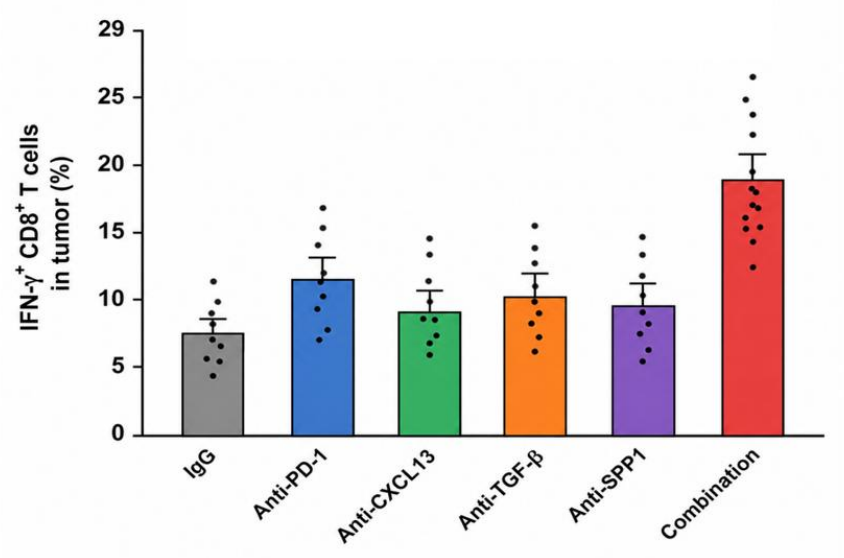

Table 4

Endpoint tumor volume and immune indicators in mouse xenograft models

Group	MC38 Tumor Volume (mm^3)	MC38 TGI（%）	B16-OVA tumor volume (mm^3)	B16-OVA TGI（%）	Exhausted $CD8^+$ T (%)	IFN-γ^+CD8^+T（%）
IgG Control	1,286.4±218.7	—	1,104.7±196.5	—	51.8±7.3	7.6±2.0
Anti-PD-1	842.6±176.3	34.5	785.2±168.4	28.9	43.2±6.6	11.4±2.7
Anti-CXCL13	993.1±189.4	22.8	902.6±181.7	18.3	46.5±6.9	9.2±2.3
Anti-TGF-β	905.8±172.6	29.6	826.9±174.2	25.1	44.8±6.7	10.1±2.5
Anti-SPP1	963.5±184.1	25.1	871.4±177.9	21.1	45.9±6.8	9.7±2.4
Anti-PD-1 Combination	436.8±102.5	66.0	456.3±109.8	58.7	24.6±5.1	18.9±4.2
P value	<0.001	—	0.003	—	<0.001	<0.001

4. Discussion

This study focuses on three questions: how exhausted T cells are spatially organized in tumor tissues, which cells and signals make up their niche, and whether they can serve as targets to enhance ICB. The main findings can be summarized in three points: exhausted T cells are not evenly distributed throughout the tumor mass but are enriched in spatial niches characterized by $SPP1^+$ tumor-associated macrophages, FAP^+ cancer-associated fibroblasts, and $FoxP3^+$ regulatory T cells; the scores based on these niches are significantly associated with lower objective response rates to anti-PD-1/PD-L1 therapy and shorter progression-free survival, and these associations can be replicated in independent external cohorts; targeting key signals in the niche such as CXCL13-CXCR5, TGF-β, and SPP1 can reverse T cell exhaustion, reshape the tumor immune microenvironment, and enhance anti-PD-1 efficacy. Overall, these results support viewing exhausted T cell niches as organized units of tumor immune suppression and provide experimental evidence for 'spatial immune remodeling' as a combinational strategy for ICB.

The cellular composition and functional state of the tumor immune microenvironment have been widely shown to be important determinants of ICB efficacy. However, previous understanding of T cell exhaustion mainly came from single-cell transcriptome studies. Such studies in liver cancer, non-small cell lung cancer, and colorectal cancer have revealed the transcriptional heterogeneity, differentiation trajectories, and potential regulatory molecules of exhausted $CD8^+$ T cells, and systematically summarized the relationship between $CD8^+$ T cell states and clinical outcomes. These

works have significantly deepened our understanding of the intrinsic programs of exhausted T cells, but because tissue dissociation loses spatial information, it is difficult to define the 'neighborhood environment' of exhausted T cells in situ or directly determine which cells they have stable interactions with. In comparison, this study builds spatial neighborhoods centered on exhausted T cells and finds that $SPP1^{+}$ macrophages, FAP^{+} fibroblasts, and regulatory T cells are significantly enriched around exhausted T cells, suggesting that T cell exhaustion is not only a change in cell state but also a process embedded in specific tissue structures. This understanding aligns with the spatial organizational heterogeneity emphasized in the 'immune-hot, altered, and cold tumors' classification framework, and also provides a new tissue-level perspective to explain differences in ICB responses within the same cancer type.

In recent years, spatial transcriptomics, multiplex immunofluorescence, and high-dimensional imaging technologies have made it possible to study immune cell neighborhoods. In breast and colorectal cancers, researchers have proposed the concept of "cell neighborhoods" and found that the way immune cells coordinate spatially is related to anti-tumor immune states and clinical outcomes. For example, Schürch et al. found that coordinated cell neighborhoods at the invasive front of colorectal cancer could organize anti-tumor immunity; Keren et al. revealed structured organization at the tumor-immune interface in triple-negative breast cancer using multiplex ion beam imaging. These studies laid the methodological foundation for spatial immune analysis, but most analyses focus on the tumor-immune interface or overall neighborhoods, without specifically defining niches centered on exhausted T cells, and they rarely systematically validate spatial features together with ICB efficacy stratification and causal interventions in the same framework. Building on this, our study advances in three ways: defining niches centered on exhausted T cells rather than tumor regions, so that spatial analysis directly reflects this key immunological process; quantifying niche composition into reproducible scores and evaluating their relationship with ORR and PFS in both discovery and external cohorts; and intervening on key niche nodes through organoid-TIL co-culture and transplant tumor models, thus moving from descriptive spatial associations to an actionable mechanistic level.

At the mechanism level, the three nodes identified in this study align well with existing evidence. TGF-β signaling has been shown to impair the efficacy of PD-L1 blockade by promoting T cell exclusion, and in this study, anti-TGF-β intervention significantly reduced the extent of the exhausted phenotype in organoid co-cultures, suggesting that TGF-β may be an important upstream signal maintaining immune suppression in the niche. The CXCL13-CXCR5 axis is involved in the spatial recruitment and organization of immune cells, and CXCL13-producing T follicular helper-like cells have been linked to immune suppression and adaptive immune memory; in this study, anti-CXCL13 intervention partially reduced the proportion of exhausted T cells, suggesting that this axis may be involved in the retention or re-recruitment of exhausted T cells in specific areas. The spatial interaction

between SPP1$^+$ macrophages and FAP$^+$ fibroblasts has been shown to shape the immunosuppressive microenvironment in colorectal cancer, and this study further shows that the two are co-enriched in the exhausted T cell niche, with combined blockade of SPP1, TGF-β, and CXCL13 being more effective than any single agent. This result suggests that the niche is not dominated by a single pathway, but rather involves network redundancy and synergistic regulation; blocking just one node may be bypassed by other compensatory signals, while combined intervention is more likely to achieve 'spatial immune remodeling.' Of course, the intervention experiments in this study still cannot distinguish the relative contributions of each node to niche formation, maintenance, and functional output, and further studies using conditional gene knockout, lineage tracing, and spatial perturbation experiments are needed to dissect the causal hierarchy.

The methodological innovation of this study mainly lies in the integration of the 'spatial immune remodeling' framework. We combined spatial transcriptomics, multiplex immunofluorescence, and single-cell RNA sequencing in the same cohort, utilizing single-cell data for cell type annotation and communication inference, while preserving in situ neighborhood information with spatial data, and cross-validating with consecutive slice multiplex immunofluorescence. Compared to studies that rely only on single-cell ligand-receptor inference, this strategy reduces the risk of mismatch between 'computationally predicted communication' and 'in situ spatial proximity.' Compared to descriptive studies based solely on tissue imaging, niche scoring provides quantitative metrics that are statistically analyzable, stratifiable, and externally verifiable. Moreover, this study was not limited to a single cancer type; we observed niche features in non-small cell lung cancer, hepatocellular carcinoma, colorectal cancer, and breast cancer, and validated their prognostic associations in independent external cohorts, enhancing the generalizability of the results. It's important to note that consistency across cancer types does not mean mechanistic homogeneity; the proportion of cells in the niche, stromal composition, and signaling weights may vary across different tumors, so future studies should conduct cancer type-specific spatial multi-omics analyses.

In terms of clinical translation, our study suggests that the spatial niche score of tumor tissue before treatment could serve as a supplementary marker for stratifying ICB efficacy. Current clinical decisions mainly rely on indicators like PD-L1 expression, tumor mutation burden, and microsatellite instability, but these markers have limited predictive power across different cancer types and treatment lines. Our study shows that the niche score correlates with ORR and PFS, and its AUC is better than that of CD8$^+$ T cell density alone, indicating that the 'spatial organization of immune cells' might provide information independent of cell abundance. If staining, scanning, and analysis processes could be standardized in prospective cohorts, this score has the potential to identify patients who might benefit less from ICB monotherapy and may need combined niche-targeted strategies. For combination strategies, anti-TGF-β, anti-CXCL13, and anti-SPP1 all showed some synergistic effects

in the models, but adverse reactions and target specificity in the combination setting still need to be evaluated in clinical trials. In particular, TGF-β has broad physiological functions, so systemic blockade may pose safety issues; future approaches could consider local delivery, bispecific antibodies, or conditionally activated drugs.

This study has several limitations. The discovery cohort is a multi-center observational cohort. Although the sample size meets the estimate for the primary endpoint, the sample sizes for each cancer subgroup are limited, making it difficult to fully assess cancer-specific effects. The external cohort is also retrospective, and selection bias and differences in follow-up could affect survival estimates. Spatial transcriptomics spots have multi-cellular resolution; although the 50 μm neighborhood radius and upper quartile threshold were set based on prior knowledge and sensitivity analyses, they could still be influenced by tissue type, cell density, and slice thickness. The reproducibility across different platforms and analytical workflows still needs to be verified in multi-center standardized studies. The multiplex immunofluorescence panels cover only a limited set of markers, so they cannot simultaneously analyze T cell exhaustion clonality, metabolic state, and antigen specificity, nor systematically assess the contributions of B cells, dendritic cells, and neutrophils. Organoid-TIL co-culture and xenograft models can provide functional evidence, but the former lacks a complete stroma and immune system, while the latter differs from human tumors in genetic background and microenvironment. Antibody blockade also cannot fully replicate genetic deletion, and off-target effects are hard to rule out. This study did not assess dynamic changes in niches after treatment, so it cannot determine whether niche scores are predictive or prognostic markers; future studies should perform longitudinal spatial analyses on paired pre- and post-treatment samples. Finally, this study did not compare niche scores head-to-head with existing clinical markers in a prospective manner, so their incremental value still needs to be verified in registered cohorts.

That said, this study still provides testable mechanistic hypotheses and translational pathways: the exhausted T cell niche may act as a ‘tissue unit’ of local immunosuppression, maintaining T cell dysfunction through the $SPP1^{+}$ macrophage–FAP^{+} fibroblast–TGF-β axis and the CXCL13–CXCR5 axis; targeting the key nodes of this niche could reshape the immune microenvironment and sensitize the response to ICB. Research could move forward in three directions: first, conduct prospective, multi-cancer spatial immune cohorts to standardize niche scoring and assess its clinical utility; combine spatial multi-omics, lineage tracing, and conditional gene editing to unravel the causal mechanisms of niche formation and maintenance; develop combinational intervention strategies targeting niche networks rather than single molecules, and assess safety and efficacy in early clinical trials.

In summary, this study advances exhausted T cells from the ‘cell state’ level to the ‘spatial niche’ level, proposing and validating the feasibility of a ‘spatial immune remodeling’ strategy. The results

not only deepen our understanding of the histological basis of tumor immune suppression but also provide new candidate biomarkers and intervention nodes for ICB efficacy stratification and combination therapy. Further validation of their translational value is needed in real-world prospective cohorts and clinical trials.

5. Conclusion

In summary, this study reveals the spatial niche characteristics of exhausted T cells in tumors from three perspectives: spatial organization, clinical correlation, and functional intervention. Exhausted T cells are not evenly distributed; instead, they are enriched in spatial niches composed of $SPP1^+$ tumor-associated macrophages, FAP^+ cancer-associated fibroblasts, and $FoxP3^+$ regulatory T cells. Scores based on these niches are significantly associated with reduced objective response rates to anti-PD-1/PD-L1 therapy and shorter progression-free survival, and these findings can be replicated in independent external cohorts. Targeting key niche signals such as CXCL13-CXCR5, TGF-β, and SPP1 can reverse T cell exhaustion, reshape the tumor immune microenvironment, and enhance the efficacy of anti-PD-1 therapy. These results support viewing the exhausted T cell niche as an organized unit of tumor immune suppression and suggest that 'spatial immune remodeling' could offer a new approach for stratifying ICB efficacy and designing combination interventions.

Future research still needs to standardize niche scoring in prospective, multi-cancer cohorts and evaluate its clinical utility; combine spatial multi-omics, lineage tracing, and conditional gene editing to understand the causal mechanisms behind niche formation and maintenance; develop combined intervention strategies targeting the niche network instead of individual molecules, and systematically assess their safety and effectiveness in early clinical trials. As spatial immune analysis technologies become standardized and clinical translation progresses, exhausted T cell niches are expected to serve as an important bridge connecting basic research on the immune microenvironment with precise ICB treatment.

Acknowledgments

The authors declare that no specific acknowledgments are required.

Author contributions

Conceptualization, Gang Liu and Jia Wang; methodology, Jia Wang; validation, Gang Liu; formal analysis, Jia Wang; investigation, Gang Liu and Jia Wang; resources, Gang Liu; data curation, Jia Wang; writing—original draft preparation, Jia Wang; writing—review and editing, Gang Liu; visualization, Jia Wang; supervision, Gang Liu; project administration, Gang Liu. All authors have read and agreed to the published version of the manuscript.

Funding

This research received no external funding.

Data availability

The supplementary materials and datasets supporting the findings of this study have been deposited in Zenodo and are publicly available at https://doi.org/10.5281/zenodo.24465320.

Declarations

Conflict of interest

The authors declare that there is no conflict of interest.

Ethics approval

Not applicable.

Consent to participate

Not applicable.

Consent for publication

All authors have given their consent.

Additional information

Received: 16 November 2026

Accepted: 16 November 2026

Published online: 23 November 2026

Publisher's Note

Wisdom Academic Press Ltd. remains neutral with regard to jurisdictional claims in published maps and institutional affiliations.

References

[1] Blank, C. U., Haining, W. N., Held, W., Hogan, P. G., Kallies, A., Lugli, E., et al. (2019). Defining "T cell exhaustion". *Nat Rev Immunol, 19*(11), 665-674. https://doi.org/10.1038/s41577-019-0221-9

[2] Cheng, S., Li, Z., Gao, R., Xing, B., Gao, Y., Yang, Y., et al. (2021). A pan-cancer single-cell transcriptional atlas of tumor infiltrating myeloid cells. *Cell, 184*(3), 792-809.e23. https://doi.org/10.1016/j.cell.2021.01.010

[3] Chevrier, S., Levine, J. H., Zanotelli, V. R. T., Silina, K., Schulz, D., Bacac, M., et al. (2017). An immune atlas of clear cell renal cell carcinoma. *Cell, 169*(4), 736-749.e18. https://doi.org/10.1016/j.cell.2017.04.016

[4] Goltsev, Y., Samusik, N., Kennedy-Darling, J., Bhate, S., Hale, M., Vazquez, G., et al. (2018). Deep profiling of mouse splenic architecture with CODEX multiplexed imaging. *Cell, 174*(4), 968-981.e15. https://doi.org/10.1016/j.cell.2018.07.010

[5] Guo, X., Zhang, Y., Zheng, L., Zheng, C., Song, J., Zhang, Q., et al. (2018). Global characterization of T cells in non-small-cell lung cancer by single-cell sequencing. *Nat Med, 24*(7), 978-985. https://doi.org/10.1038/s41591-018-0045-3

[6] Gu-Trantien, C., Migliori, E., Buisseret, L., de Wind, A., Brohée, S., Garaud, S., et al. (2017). CXCL13-producing TFH cells link immune suppression and adaptive memory in human breast cancer. *JCI Insight, 2*(11), e91487. https://doi.org/10.1172/jci.insight.91487

[7] Jackson, H. W., Fischer, J. R., Zanotelli, V. R. T., Ali, H. R., Mechera, R., Soysal, S. D., et al. (2020). The single-cell pathology landscape of breast cancer. *Nature, 578*(7796), 615-620. https://doi.org/10.1038/s41586-019-1876-x

[8] Mariathasan, S., Turley, S. J., Nickles, D., Castiglioni, A., Yuen, K., Wang, Y., et al. (2018). TGFβ attenuates tumour response to PD-L1 blockade by contributing to exclusion of T cells. *Nature, 554*(7693), 544-548. https://doi.org/10.1038/nature25501

[9] McLane, L. M., Abdel-Hakeem, M. S., & Wherry, E. J. (2019). CD8 T cell exhaustion during chronic viral infection and cancer. *Annu Rev Immunol, 37*, 457-495. https://doi.org/10.1146/annurev-immunol-041015-055318

[10] Qi, J., Sun, H., Zhang, Y., Sun, Z., Wang, J., Liu, X., et al. (2022). Single-cell and spatial analysis reveal interaction of FAP+ fibroblasts and SPP1+ macrophages in colorectal cancer. *Nat Commun, 13*(1), 1742. https://doi.org/10.1038/s41467-022-29366-6

[11] Qian, J., Olbrecht, S., Boeckx, B., Vos, H., Laoui, D., Etlioglu, E., et al. (2020). A pan-cancer blueprint of the heterogeneous tumor microenvironment revealed by single-cell profiling. *Cell Res, 30*(9), 745-762. https://doi.org/10.1038/s41422-020-0355-0

[12] Schürch, C. M., Bhate, S. S., Barlow, G. L., Phillips, D. J., Noti, L., Zlobec, I., et al. (2020). Coordinated cellular neighborhoods orchestrate antitumoral immunity at the colorectal cancer invasive front. *Cell, 182*(5), 1341-1359.e19. https://doi.org/10.1016/j.cell.2020.07.005

[13] Sharma, P., Hu-Lieskovan, S., Wargo, J. A., & Ribas, A. (2017). Primary, adaptive, and acquired resistance to cancer immunotherapy. *Cell, 168*(4), 707-723. https://doi.org/10.1016/j.cell.2017.01.017

[14] Ståhl, P. L., Salmén, F., Vickovic, S., Lundmark, A., Navarro, J. F., Magnusson, J., et al. (2016). Visualization and analysis of gene expression in tissue sections by spatial transcriptomics. *Science, 353*(6294), 78-82. https://doi.org/10.1126/science.aaf2403

[15] Stickels, R. R., Murray, E., Kumar, P., Li, J., Marshall, J. L., Di Bella, D. J., et al. (2021). Highly sensitive spatial transcriptomics at near-cellular resolution with Slide-seqV2. *Nat Biotechnol, 39*(3), 313-319. https://doi.org/10.1038/s41587-020-0739-1

[16] Thommen, D. S., & Schumacher, T. N. (2018). T cell dysfunction in cancer. *Cancer Cell, 33*(4), 547-562. https://doi.org/10.1016/j.ccell.2018.03.012

[17] Thommen, D. S., Koelzer, V. H., Herzig, P., Roller, A., Trefny, M., Dimeloe, S., et al. (2018). A transcriptionally and functionally distinct PD-1+ CD8+ T cell pool with predictive potential in non-small-cell lung cancer treated with PD-1 blockade. *Nat Med, 24*(7), 994-1004. https://doi.org/10.1038/s41591-018-0057-z

[18] Topalian, S. L., Drake, C. G., & Pardoll, D. M. (2015). Immune checkpoint blockade: A common denominator approach to cancer therapy. *Cancer Cell, 27*(4), 450-461. https://doi.org/10.1016/j.ccell.2015.03.001

[19] Tumeh, P. C., Harview, C. L., Yearley, J. H., Shintaku, I. P., Taylor, E. J., Robert, L., et al. (2014). PD-1 blockade induces responses by inhibiting adaptive immune resistance. *Nature, 515*(7528), 568-571. https://doi.org/10.1038/nature13954

[20] Wherry, E. J. (2011). T cell exhaustion. *Nat Immunol, 12*(6), 492-499. https://doi.org/10.1038/ni.2035

[21] Zhang, L., Yu, X., Zheng, L., Zhang, Y., Li, Y., Fang, Q., et al. (2018). Lineage tracking reveals dynamic relationships of T cells in colorectal cancer. *Nature, 564*(7735), 268-272. https://doi.org/10.1038/s41586-018-0694-x

[22] Zhang, Q., He, Y., Luo, N., Patel, S. J., Han, Y., Gao, R., et al. (2019). Landscape and dynamics of single immune cells in hepatocellular carcinoma. *Cell, 179*(4), 829-845.e20. https://doi.org/10.1016/j.cell.2019.10.003

[23] Zheng, C., Zheng, L., Yoo, J.K., Guo, H., Zhang, Y., Guo, X., et al. (2017). Landscape of infiltrating T cells in liver cancer revealed by single-cell sequencing. *Cell, 169*(7), 1342-1356.e16. https://doi.org/10.1016/j.cell.2017.05.035